Research Article | Vol. 10, No. 11 / 1 November 2019 / Biomedical Optics Express 6009
Biomedical Optics EXPRESS

Imaging relative stasis of the blood column in human retinal capillaries

PHILLIP BEDGGOOD* AND ANDREW METHA

Department of Optometry and Vision Sciences, The University of Melbourne, 3010, Australia
*pabedg@unimelb.edu.au

Abstract: Capillary flow largely consists of alternating red cells and plasma whose speed oscillates predictably with the cardiac cycle. Superimposed on this regular background are sporadic events potentially disruptive to capillary exchange: the passage of white cells, aggregates of red cells, epochs of sparse haematocrit, or unusually slow flow. Such events are not readily differentiated with velocimetry or perfusion mapping. Here we propose a method to identify these phenomena in retinal capillaries imaged with high frame-rate adaptive optics, by calculating and representing pictorially the autocorrelation of intensity through time at each pixel during short epochs. The phenomena described above manifest as bright regions which transiently appear and propagate across an otherwise dark image. Drawing data from normal subjects and those with Type I diabetes, we demonstrate proof of concept and high sensitivity and specificity of this metric to variations in capillary contents and rate of flow in health and disease. The proposed metric offers a useful adjunct to velocimetry and perfusion mapping in the study of normal and abnormal capillary blood flow.

© 2019 Optical Society of America under the terms of the OSA Open Access Publishing Agreement

1. Introduction

With adaptive optics (AO) it is possible to image the microvascular networks of the retina in living human eyes, allowing observations of capillary structure and perfusion [1,2]. With high speed it is possible to track individual red cells, white cells, platelets and lengths of plasma as they traverse the network [3–6]. Such approaches offer a uniquely non-invasive "window" to the internal microvasculature of the body, in particular that located within neural tissue, which is not afforded by other investigative means. This technology is therefore well placed to study pathological processes observed or initiated at the level of the smallest vessels, which have been implicated in a broad spectrum of diseases affecting multiple sites across the body including diabetes, hypertension, sickle cell disease, coronary heart disease, cerebral ischemia, stroke and dementia [7–10].

The high spatial and temporal resolution afforded by AO offer the potential for exquisite sensitivity to early pathological changes which may be missed by other assays. Previous work has demonstrated structural vascular adaptations including altered branching [11], tortuosity [12,13], wall thickening with narrowing of the lumen [12,14–17], and the formation of overt microstructural abnormalities such as microaneurysms [18,19]. In many cases these are detectable prior to pathology observable on standard clinical examinations.

A fundamental outstanding question is whether such structural adaptations themselves occur secondary to the formation of abnormal patterns of flow. There is reasonable evidence from AO imaging studies to suggest this as a plausible theory: the formation and resolution of structurally intact "ghost" vessels [12,20–22]; diversion of leukocytes from their preferred paths [13,23]; more rapid aggregation of erythrocytes [24]; and greater heterogeneity in capillary flow [24] have all been noted in diabetes in the absence of structural abnormalities. This evidence accords with previous reports of faster flow for large retinal vessels early in diabetes, followed later by slowed flow concomitant with clinically observed structural changes [25,26].

#377702 https://doi.org/10.1364/BOE.10.006009
Journal © 2019 Received 11 Sep 2019; revised 21 Oct 2019; accepted 22 Oct 2019; published 1 Nov 2019

Biomedical Optics EXPRESS

The impact of any challenge to normal perfusion of the microvascular network is likely to be highly dynamic. In addition to network redundancy and large natural variations in rate of flow and capillary contents [4], vessels as small as individual capillaries can actively constrict and dilate in line with local neuronal activity [27]. Dysfunction of this regulatory response has been indicated in many disease entities [9]. Hence, pathological flow states arising in any single vessel may spontaneously resolve, or else spread their influence to adjacent vessels depending on prevailing conditions [28]. Flow patterns early in disease may therefore transition from a state of normality, through intermittent periods of abnormality, and finally into a consistently abnormal state. Accordingly, it is of central importance to be able to identify those brief periods where flow begins to enter an aberrant state. This would advance fundamental understanding of pathophysiology and offer sensitive diagnostic assessment of microvascular dysfunction.

Recently developed methods allow quantification of flow velocity over short epochs (e.g. 100 ms) in select vessels and/or across the imaged field, potentially allowing identification of intermittently pathological flow states [29–32]. Studies to date have shown marked variability of flow both within and between vessels at all levels of the retinal microvasculature. This is driven by changes in blood pressure across the cardiac cycle as well as stochastic dependency on cell "traffic" negotiating a complex network. These sources of variability make the identification of abnormal flow epochs challenging. In addition, simple velocity mapping does not generally provide unambiguous analysis of the constituents of the blood column (though it can be done well when targeting individual capillaries [5,32]). This information is required to inform hypotheses regarding the metabolic impact of flow alterations; for example, slowed flow in a vessel of high haematocrit may preserve sufficient oxygen exchange with tissue, and conversely a vessel of fast flow but low haematocrit may not.

In the present work we present a new and simple metric for the analysis of capillary flow data which compliments existing velocity mapping approaches. The metric can be thought of as a "decay time" for each pixel and is calculated from the frequency spectrum of individual pixels, within short (100 ms) epochs in time. Decay time is shown to increase in cases of relative "stasis" of the blood column, which we use here to identify periods of slowed flow, low haematocrit, and the passage of cell aggregates and/or white blood cells, each of which are relevant to instantaneous efficiency of metabolite exchange. We utilised outlier analysis on the decay time metric to flag "interesting" events in each vessel, and manually reviewed the flagged events to demonstrate how the new metric can be interpreted. We also present data from young diabetic eyes without any clinically detected retinopathy, which appear to show periods of pronounced stasis.

2. Methods

2.1. Subjects

This study was aligned with the tenets of the Declaration of Helsinki and approved by the University of Melbourne Human Ethics Committee. Subjects provided written informed consent prior to all testing.

We retrospectively reviewed data from 5 normal subjects (age 22-23 years) with no known medical issues, and 10 subjects with Type I diabetes (age 18-31 years). Data were selected for analysis based on optical quality and stability of fixation; 2/5 normal subjects and 8/10 diabetic subjects were chosen in this way. Two subjects in each group were excluded due to poor image quality resulting from intraocular scatter; one normal subject was excluded due to fixation of insufficient quality to obtain measurements over multiple cardiac cycles. For the diabetics we present data anecdotally; sequences were selected which captured clearly elevated decay time within the brief acquisition period (400 ms), co-occurring with micro-structural pathology in the field (data from 3 subjects shown).

Normal subjects were recruited from staff and students in the Department of Optometry and Vision Sciences from the University of Melbourne. Diabetic subjects were recruited from

Biomedical Optics EXPRESS

Ophthalmology at Royal Melbourne Hospital and did not have any retinopathy observed from colour fundus photography. HbA1c and blood glucose levels at the time of imaging were not ascertained.

2.2. Image acquisition

A flood-illumination adaptive optics ophthalmoscope was used to image the retinal capillary network over a 1.25° field, as described recently [29]. Pixels are exposed simultaneously and illuminated with 50% duty cycle (global shutter) at different frame rates and imaging wavelengths as described below. Locations imaged were within 1-3° from fixation. In this region there is little stratification of retinal capillary plexi, which obviates the need to obtain and combine data from multiple planes of focus.

For the normal subjects we sought to obtain information over multiple cardiac cycles, leading to the use of a longer imaging wavelength (750 nm) to facilitate steady fixation during a 3.3 second imaging period at 300 fps.

Data from the diabetic eyes was originally intended primarily for structural analysis, hence we used a light better absorbed by haemoglobin (593 nm) which is too bright for fixation to be maintained over long periods. Thus individual movie sequences were limited in duration to 400 ms at 200 fps.

2.3. Image processing

Prior to calculation of the decay time metric, acquired sequences were background-subtracted and flat-fielded as described previously [29]. Eye movements (image translations) were compensated by Fourier-based cross-correlation, which provides robust sub-pixel precision for flood illumination imaging since there is no inter-frame distortion [33]. Correction for translation was generally excellent, due to the imaged vessel structure and mottled appearance of the out-of-focus cone mosaic. Rotation correction within sequences was found to be unnecessary. Quality of registration for each frame was assessed manually, and can be confirmed by the reader through inspection of the included sequences.

For the standard deviation and decay time images shown here, and for calculation of velocity maps, for each pixel a rolling average intensity was calculated within a 200 ms epoch and subtracted from the intensity of that pixel. This acts to suppress structural information and promote changes over time (specifically, changes within a 200 ms epoch). The 200 ms epoch was chosen to be twice the duration of the epoch over which decay time and velocity were calculated (100 ms, based on previous work [29,31,34]). Following subtraction of the rolling average, again for each pixel, a linear trend in pixel intensity was fit and subtracted from the entire data sequence, largely to minimise changes over time due to background bleaching of photopigment when imaging at 593 nm.

2.4. Calculation of decay time

Figure 1 illustrates calculation of the decay time metric, which operates for each pixel in the image independently. Average intensity data for an acquired sequence is shown in Fig. 1(A). After normalization of each pixel to the frame mean, followed by subtraction of the mean intensity in a rolling temporal window as described above, "normalized" intensity is obtained (shown in Fig. 1(B) for two example pixels). If a pixel, identified as representing part of a blood vessel, tends to retain its intensity over time there are two potential explanations: slow flow, or unchanging capillary contents which indicate a long plasma column (low haematocrit) or a long cell column (indicating red cell aggregates or a white blood cell). To quantify how this "persistence" in the intensity signal becomes degraded in time for each pixel, its autocorrelation was calculated. An autocorrelation function which drops off rapidly would indicate, for example, faster flow and/or higher haematocrit at that pixel. To condense this function to a single number, we calculated the

Biomedical Optics EXPRESS

centroid of its frequency spectrum (Fig. 1(E)). The inverse of this centroid can be considered as a "decay time" for the intensity information at that pixel; this allows a "decay time image" to be populated (Fig. 1(F)) for the epoch in question.

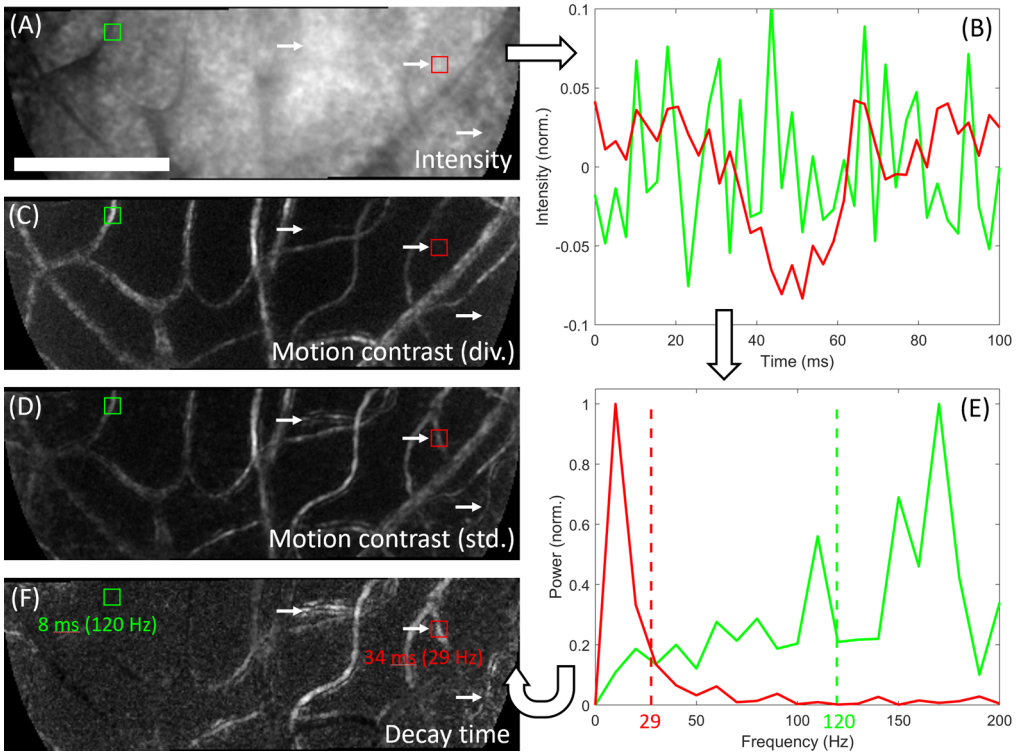

Fig. 1. Calculation of the decay time image, illustrated with data from a human subject with Type I diabetes. Image sequence acquired at 400 fps with 593 nm light ~2° from fixation. Data is separated into 100 ms epochs for analysis and each pixel considered independently; the figure shows one such epoch. A) Average pixel intensity. Red and green squares indicate 2 example pixels, and white arrows indicate 3 example vessels. B) Plot of intensity for the example pixels. The green pixel varied rapidly while the red pixel changed more slowly. C) Motion contrast calculated by the "division" method. The example vessels (white arrows) appear either dim or not visible at all. D) Motion contrast calculated by the standard deviation method. All indicated vessels appear visible. E) Intensity data is used to compute the Fourier transform of the autocorrelation function (or equivalently, the power spectrum). Dashed vertical lines indicate the centre of gravity for each pixel; centroids in frequency space are inverted to the time domain and used to populate the decay time image, shown in F). Bright vessels in the decay time image result from sluggish flow and/or low haematocrit; especially of note are the indicated vessels (white arrows) which did not appear on the division image. The flow in these vessels during this epoch can be inspected directly in Visualization 1. Images are linearly stretched to fill an 8-bit colormap; decay time values shown range from 7 to 35 ms. Scale bar is 100 μm.

If the signal mean, variance and autocorrelation itself do not change appreciably over the epoch analysed, according to the Wiener-Khinchin theorem the Fourier transform of the autocorrelation function (which we described above) is equivalent to the power spectrum. In our data we have observed negligible error when decay time is calculated from the latter instead of the former; since the power spectrum is faster to calculate, all decay time data presented in this paper are derived from the (inverse of the centroid of the) power spectrum.

Biomedical Optics EXPRESS

Also shown in Fig. 1(C) and 1(D) are motion contrast images generated by "division" [2] or standard deviation [1] methods . These panels illustrate the difficulty of relying on one method to generate a vascular perfusion map; although vessels appear sharper in the division image, there are several invisible or barely visible vessels (white arrows) which appear in the standard deviation image. As revealed by inspection of the accompanying sequence (Visualization 1), these vessels showed slowed flow and/or low haematocrit. Accordingly these vessels, which happen to come from a subject with Type I diabetes, appear bright in the decay time image (Fig. 1(F)).

2.5. Calculation of velocity

To help interpret variations in the decay time signal within each vessel, we computed the flow velocity during the same epochs using pixel intensity cross-correlation. This has been described in full recently [29]; essentially, estimates of velocity are calculated for individual pixels by finding the most correlated nearby pixel after the intensity data is shifted forwards or backwards in time by one frame. When averaged over whole vessel segments i.e. many pixels, the measured velocity is robust.

2.6. Image segmentation

To ascribe a decay time or velocity value to a given vessel segment, pixel values within each segment were averaged. Our procedure for vessel segmentation was detailed recently [29] and is summarised below.

To identify individual segments, the "division" motion contrast image was calculated to highlight vascular lumens. A vesselness filter [35] was applied with a nominal diameter of 5 μm, and then binarized using Otsu's method. The output of this procedure was skeletonized, branch points were removed, and segments lengths <20 μm were discarded. This allowed a unique identifier to be assigned to the skeletonized centreline of each vessel segment.

To determine vessel diameters we formed a cross-section of the motion contrast signal perpendicular to each vessel [27]; this was averaged (collapsed) down the length of the vessel, and thresholded by Otsu's method to locate the (average) vessel edges. It should be noted that segments highlighted in figures have a diameter 2.0 μm greater than this, so as not to obscure the edge of the vessel; this is relevant to examples given below where areas of elevated decay time appear outside the nominal vessel lumen.

2.7. Outlier pixels and the "sheath" index

The results will present the novel observation that at certain times, the intensity of pixels several microns from the nominal vessel lumen can be influenced by variations in capillary contents and flow dynamics. This influence could be physical (for example, plasma swelling to pass a blockage) or optical (for example, a difference in scattering properties between cells and plasma in conjunction with the double-pass passage of light), or some combination thereof.

To assign pixels of high decay time to the proximal vessel, we identified outlier image pixels using the default settings of the Matlab 2018a "isoutlier" function, which flags pixels with intensity differences greater than 3 scaled median absolute deviations from the median. Contiguous clusters of outlier pixels, numbering 5 or more, which abutted or overlapped a nominal vessel lumen were assigned to that vessel. Reported and plotted decay time values do not include this process (it was used only to identify outliers). However, we did record the proportion of additional pixels that could be assigned to each vessel in this way, which forms the "sheath" index in Table 1.

Biomedical Optics EXPRESS

2.8. Outlier epochs

Pixels assigned to a given vessel segment were averaged to arrive at a single decay time value for that segment during each recorded epoch. To show the utility of the decay time metric we reviewed "unusual" values for each segment, by flagging them using the same "isoutlier" function described above. Three classes of outlier epochs were assessed:

- "Outlier-to-self": relative to typical values for the vessel obtained over multiple cardiac cycles, e.g. detecting the passage of a cell aggregate in a vessel which does not usually permit them.
- "Outlier-to-field": relative to all the other segments in the field, i.e. detecting decay time that is elevated given the present phase of the cardiac cycle and local network "traffic".
- "Outlier-given-velocity": relative to all segments and epochs in the sequence which had similar velocity (binned in 0.25 mm/sec increments), e.g. detecting a long cell aggregate which moves through a high-speed vessel.

2.9. Blinded review of outlier epochs

Outlier epochs flagged according to one or more of the above conditions were reviewed manually to classify the capillary contents during the epoch. To minimize bias, an equal number of "control" epochs were selected at random from the remaining segments and interspersed in a blinded, randomised fashion for manual review. For each vessel-epoch reviewed, a 200 ms movie was played, with a 50 ms lead-in and lead-out either side of the 100 ms epoch to provide further context. The frame rate for playback was typically 20 fps, but could be sped up or slowed down as desired.

The reviewer categorised capillary contents as follows:

- "cell(s)" : unusually long or dense cellular material indicating a white cell and/or red cell aggregate; and/or
- "plasma": unusually low haematocrit was apparent; or
- "neither": capillary contents did not appear abnormal (single file alternating flow)

Additional categorisations were made in order to exclude low quality data:

- "extended": an extended object was evident, but it was unclear whether it was cells or plasma
- "unsure": insufficient data quality to assess capillary contents at all (e.g. blur, low contrast, edge of field, change in depth leading to inversion of defocus phase contrast [34], etc)
- "segmentation error": the flagged segment was not a true vessel segment, and was removed from further analysis. Segmentation errors typically occurred as a result of thresholding (a vessel with low contrast becoming fragmented when a single fixed threshold is applied to the image) or as a result of the vesselness filter (which tends to blur nearby parallel vessels together, and somewhat suppresses crossings/junctions as these are not very "tube-like" geometries).

Flagged epochs which showed normal capillary contents (the "neither" category above) may indicate sluggish flow, or could be false positives. Rather than rely on subjective evaluation of flow speed we used the objectively determined velocity for the segment during the identified epoch. A somewhat arbitrary criterion of 1 mm/sec was applied to demarcate sluggish flow from normal flow (this condition was met in $<2\%$ of control epochs).

Biomedical Optics EXPRESS

The exclusion categories described above were selected more often for controls than for outliers; to identify an outlier generally requires a sufficient number of "clean" data points, meaning that the data from that vessel is less likely to be judged as being of poor quality. Hence the total number of outlier epochs reported in Table 1 (n = 522) was higher than the number of control epochs (n = 395); however, we regard the high number of control epochs to be sufficiently high for the testing of statistical inferences reported below.

3. Results

The most common flow condition was the regular alternating passage of red cells separated by plasma gaps. Relative to this baseline state, the decay time metric was elevated with a slowdown and/or "lengthening" of capillary contents, as expected. A "lengthening" could include a white cell, red cell aggregate, high haematocrit or low haematocrit. Such events were often but not always associated with slowed flow; conversely, slowed flow was observed both with and without an apparent change in capillary contents. We begin by providing several illustrative examples before presenting data on the manual classification of flagged epochs.

3.1. Examples

Figure 2 shows examples of transiently elevated decay time associated with a long cell aggregate and with an uninterrupted column of plasma (i.e. transient low haematocrit). Data was collected over 3.3 seconds at 300 fps. The motion contrast map is shown in Fig. 2(A), with 2 vessel segments of interest labelled ("g", "h") and highlighted (magenta). The average decay time during the sequence is shown in Fig. 2(B); both segments appear dark (low average decay time), however, decay time outliers were identified for both segments for individual epochs within the sequence.

A single (processed) frame from one such epoch is shown in Fig. 2(C); scrutiny of the movie sequence (Visualization 2) shows a long cell aggregate which creates a dark appearance (with a white "shadow") towards the right of the labelled segment, followed by an uninterrupted column of plasma which appears white with a black "shadow" (i.e. the contrast profile is inverted with the change in capillary contents). The corresponding decay time image for this epoch is shown in Fig. 2(E), showing much higher decay time than the field. Flow metrics for this segment are plotted in Fig. 2(G); the velocity (solid blue), the expected velocity (dashed blue, based on the average speed of flow through all vessels during the movie) and the decay time (red). For much of the sequence, the velocity conforms closely to the expected cardiac-derived pattern. The decay time metric appears largely as a "flatline", which is a result of high flow speed in this vessel which is insufficiently sampled by the decay time metric at 300 fps. However, at the epoch indicated by the black arrow, which corresponds to Fig. 2(C) and Fig. 2(E), flow becomes slow enough to be sufficiently sampled, producing a local peak in decay time. This has been flagged as an outlier (an "outlier-to-self", since this is not typical for the vessel; and an outlier-to-field since decay time is much higher than the rest of the field at this time).

Figure 2(D) shows a single processed frame from an earlier epoch in the same sequence (at t≈0.6s; epoch shown in Visualization 3); a long, bright section of plasma is seen within the labelled capillary segment. This is associated with elevated decay time as seen in Fig. 2(F); there is a curious pattern whereby the elevation of decay time flanks the apparent vessel lumen (the centre of the lumen appears dark). This pattern was also evident for much of segment g in Fig. 2(E). For segment h, velocity and decay time are plotted in Fig. 2(H); this vessel is seen to conform closely to the expected cardiac output, with flow velocity barely impacted by the episode of low haematocrit.

Figure 3 shows further illustrative examples for two segments "g" and "h" labelled in Fig. 3(A). Data during one example epoch is shown in Fig. 3(C), where a long, dark cell aggregate is seen just leaving the left (venous) side of segment "g", as can be observed in Visualization

Biomedical Optics EXPRESS

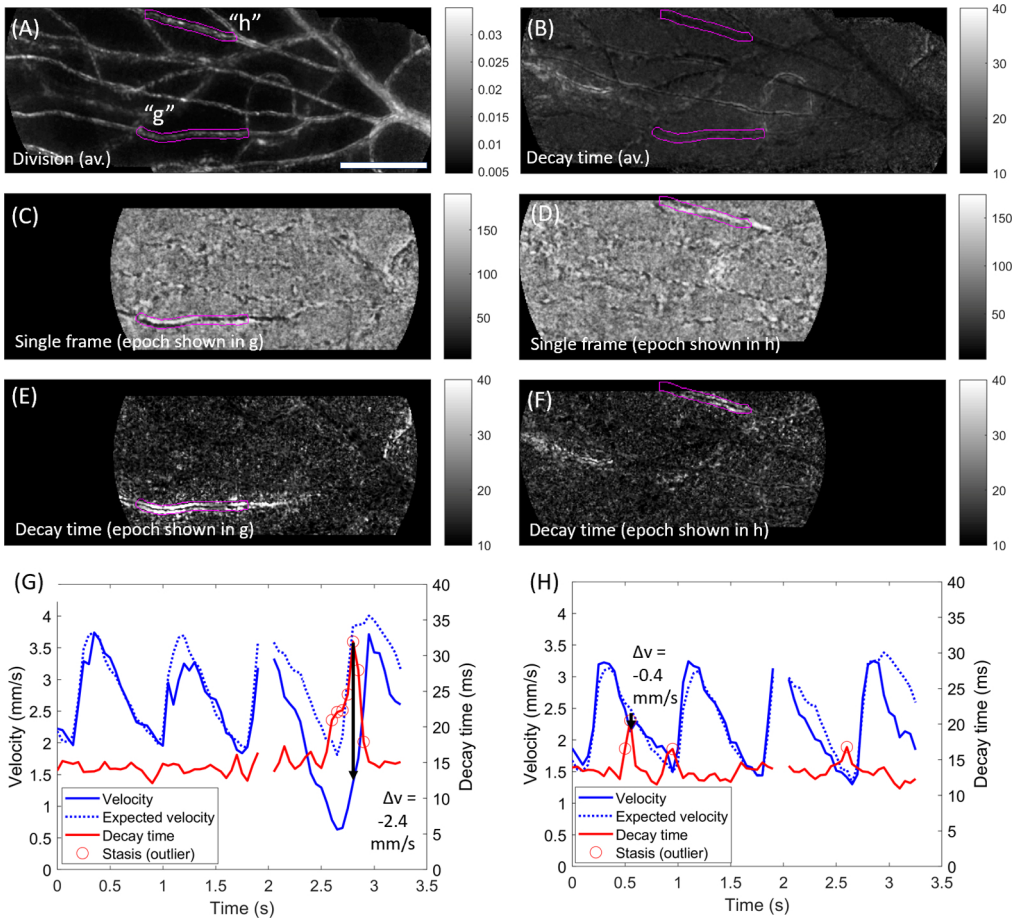

Fig. 2. Example of long, slowly moving capillary contents. Data acquired over 3.3 sec at 300 fps with 750 nm light, ~1.5° from the foveal centre in a healthy subject. A) Motion contrast (division image) for this sequence, with two vessel segments of interest labelled ("g", "h") and highlighted in magenta. B) Average decay time metric for this sequence; neither example segment had elevated decay time on average. C) Single processed frame from an example epoch (at time t≈2.8s). Within the vessel segment of interest (magenta), a chain of red cells to the right creates a black appearance (with a white "shadow" underneath); a length of plasma creates the reverse appearance on the left. The flow characteristics are best appreciated in Visualization 2. D) Single processed frame from another example epoch (at t≈0.6s). Within the vessel of interest (magenta), an uninterrupted column of plasma can be seen (refer to Visualization 3). E) Decay time image for the epoch corresponding to C, showing marked elevation of decay time in the highlighted vessel. F) As for E, but for the epoch corresponding to D. G) Evolution of flow velocity (blue) and decay time (red) for vessel "g". Expected velocity based on the field average is indicated (dashed blue). Black arrow corresponds to the epoch in C and E, and shows a pronounced drop in velocity associated with passage of the long cell aggregate. Outliers in decay time are indicated (circles). H) As for G, but data corresponds to segment "h", and the black arrow corresponds to the epoch shown in D and F. The long chain of plasma was associated with a spike in decay time but minimal disruption to velocity. Scale bar is 100 μm.

Biomedical Optics EXPRESS

4. The corresponding decay time image during this epoch is shown in Fig. 3(E), with bright pixels (elevated decay time) associated with this segment (and connecting segments) while the rest of the field appears dark. Notably, there are many bright pixels outside the nominal vessel lumen (it should be reiterated that the magenta label already extends 1 μm in each direction outside the segmented lumen; thus the extent of "bleed" does seem to extend well outside the apparent lumenal area). Flow metrics for this segment are plotted in Fig. 3(G); the velocity (solid blue), the expected velocity (dashed blue) and the decay time (red). Flagged outliers in decay time are indicated (red circles). For much of the sequence, the velocity conforms closely to the expected cardiac-derived pattern. At the black arrow close to the expected systolic peak, which corresponds to Fig. 3(C) and 3(E), velocity is slowed by approx. 1.1 mm/s from the expected value; this corresponds to an outlier in the decay time plot (in this case, it was an outlier-to-self, because it rises sufficiently above the typical variation for this vessel, as well as an outlier-to-field since it is the only bright part of the field).

Figure 3(D) shows a single frame from a different epoch in the same sequence. As opposed to the cell aggregate that was evident in Fig. 3(C), Fig. 3(D) shows a single red cell within the capillary tube surrounded by extended lengths of plasma on each side; i.e. there is low haematocrit locally. This can be verified by inspection of the accompanying sequence, Visualization 5. Corresponding elevation of the decay time metric is seen in Fig. 3(F) and, unlike Fig. 3(E), the bright pixels do not appear to extend beyond the apparent lumen. Flow metrics shown in Fig. 3(H) reveal excellent conformation of segment velocity to the expected velocity (i.e. a strong cardiac imprint), however, many epochs are flagged as outliers in decay time; these were outliers-to-field due to the low haematocrit, as opposed to outliers-to-self (the vessel consistently had low haematocrit). Negative correlation between velocity and decay time is apparent; this is expected where there is a) little change in capillary contents despite changes in velocity, and b) flow that is sufficiently slow as to be sampled adequately by single pixels (if flow is too fast we would instead see a "flatline" as seen in Fig. 3(G)).

Whereas Figs. 2 and 3 showed disruption of velocity with the presence of cell aggregates, and normal velocity in the presence of low haematocrit, Fig. 4 displays the reverse pattern (as well as showing a segment with slowed velocity in the absence of a change in contents). Here segment "e" is seen to contain a long, dark cell aggregate (Fig. 4(B)) which is associated with very high decay time (Fig. 4(C)) but minimal disruption to expected velocity at the corresponding epoch (black arrow in Fig. 4(E)). This segment is seen in fact to have high average decay time (Fig. 4(D)) which results from frequent "spikes" in decay time that are flagged as outliers (Fig. 4(E)). On some occasions these spikes are associated with slowed velocity (e.g. first and third systolic peaks), while at other times there is minimal disruption to velocity (e.g. second and fourth systolic peaks, as well as the example epoch at the black arrow). Notably, areas of elevated decay time can extend far outside the nominal lumen (magenta outline in Fig. 4(C)).

In segment "f" is seen an elongated column of bright plasma (Fig. 4(B)), in fact extending a long way into the segment above. This is associated with elevated decay time (Fig. 4(C)) which is not typical for this vessel (average decay time shown in Fig. 4(D); plot of decay time in Fig. 4(F)). Unlike the low haematocrit example of Fig. 3, low haematocrit in this vessel elevates decay time well beyond the vessel lumen (Fig. 4(C), compare magenta outline to bright pixels). The flow velocity is seen to conform at times to the expected pattern (Fig. 4(F); first systolic peak and diastolic trough) but is substantially disrupted at other times, such as at the indicated epoch (black arrow) which is associated with an outlier peak in decay time.

Along segment "g" a typical alternating light and dark pattern is seen (Fig. 4(B)), corresponding to single-file alternating flow of single cells and plasma gaps; yet decay time is elevated (Fig. 4(C) and Fig. 4(G)) and there is a substantial drop in flow velocity (Fig. 4(G)). Contrary to the other examples, which appear to be explained by what is happening locally within the segment, this pattern of a slowdown-with-normal-contents appears to result from "traffic" encountered elsewhere

Biomedical Optics EXPRESS

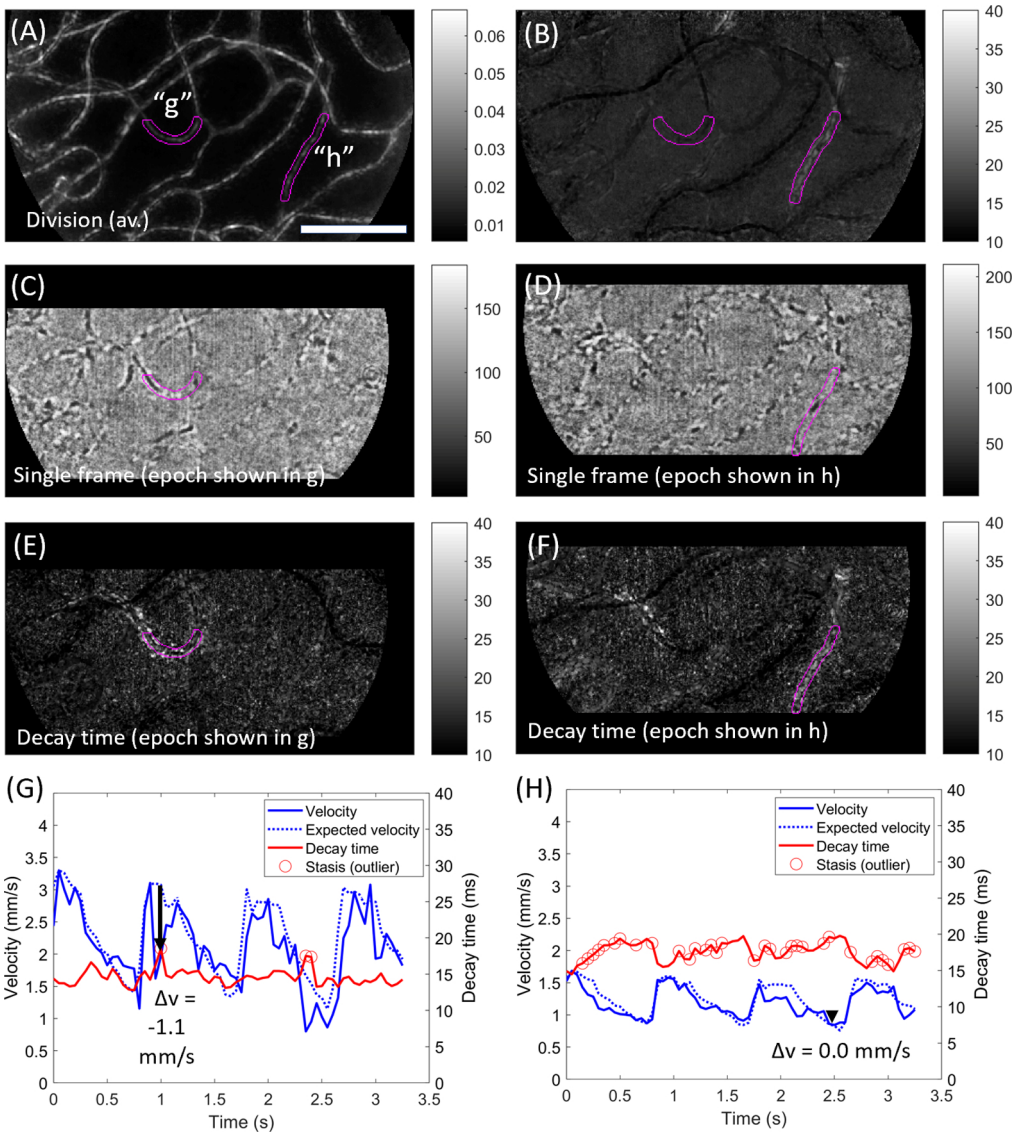

Fig. 3. Examples of a shorter cell aggregate and of a vessel with consistently low haematocrit. Data acquired over 3.3 sec at 300 fps with 750 nm light, ~2° from the foveal centre in a healthy subject. A) Motion contrast (division image) for this sequence, with two vessels of interest labelled ("g", "h") and highlighted in magenta. B) Average decay time metric for this sequence. Vessel h shows elevated decay time on average, whilst vessel g does not. C) Single processed frame from an example epoch (at t≈1.0s). Within the vessel of interest (magenta), a cell aggregate is seen exiting the left (venous) side of the segment. D) Single processed frame from another example epoch (at t≈2.5s). Within the vessel of interest (magenta), a long section of plasma is broken up by a single red blood cell, i.e. the local haematocrit is low. The flow characteristics for each example are best appreciated in Visualization 4 and Visualization 5 for segments g and h, respectively. E) Decay time image for the epoch corresponding to C. F) Decay time image for the epoch corresponding to D. G) Evolution of flow velocity (blue) and decay time (red) for vessel "g". Expected velocity based on the field average is indicated (dashed blue). Black arrow corresponds to the epoch in C and E, and shows a pronounced drop in velocity. Outliers in decay time are indicated (circles). H) As for G, but data corresponds to segment "h". The decay time metric varied inversely to the flow velocity. There are many outliers because decay time in this vessel is consistently elevated. Scale bar is 100 μm.

Biomedical Optics EXPRESS

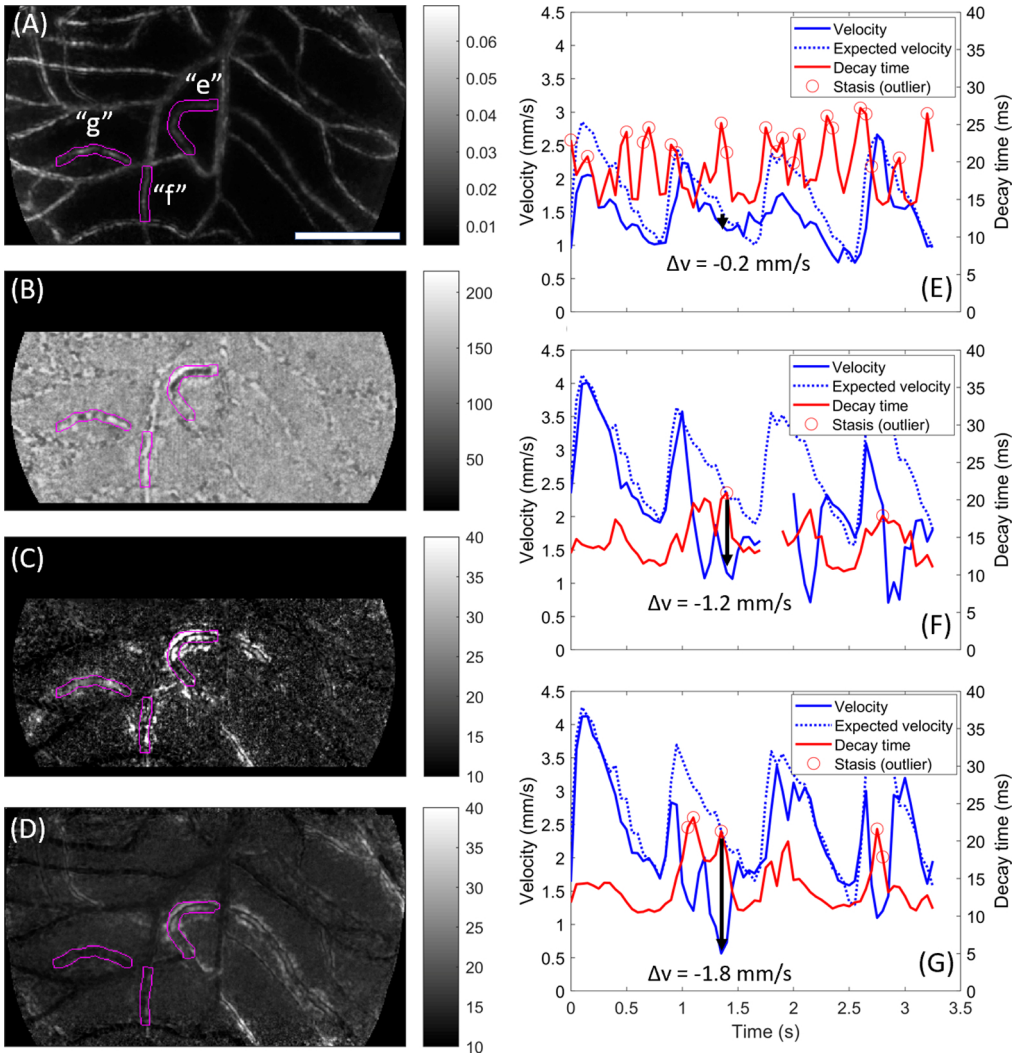

Fig. 4. Examples of the three categories of stasis captured during a single epoch. Data acquired over 3.3 sec at 300 fps with 750 nm light, 1.5° from the foveal centre in a healthy subject. A) Motion contrast (division image) for the sequence, with 3 vessels of interest labelled ("e", "f", "g") and highlighted in magenta. B) Single processed frame from an example epoch (at t≈1.4s). In segment e, a cellular aggregate creates a dark appearance. In segment f, an uninterrupted column of plasma creates a bright appearance, which extends significantly along the segment above. In segment g the capillary shows typical single file alternating flow; these observations can be verified in Visualization 6. C) Decay time image for the same epoch corresponding to B, which shows elevated decay time within and, notably, around all 3 vessels of interest. D) Average decay time metric for this sequence. Segment e shows consistently elevated decay time; segments f and g do not. E) Evolution of flow velocity (blue) and decay time (red) for segment e. Expected velocity based on the field average is indicated (dashed blue). Black arrow corresponds to the example epoch; minimal change from expected velocity is noted here despite a spike in the decay time. Outliers in decay time are indicated (circles). F) Plot for segment f, as per panel E. The extended plasma length noted in the example epoch was associated with a significant drop in velocity (black arrow). G) Plot for segment g, as per panel E. Velocity is slowed significantly from the expected value despite normal capillary contents; inspection of Visualization 6 reveals this is associated with "traffic" due to passage of the cell aggregate in segment e (segments e and g feed into the same collecting segment). Scale bar is 100 μm.

Biomedical Optics EXPRESS

within the network. Specifically, segment "g" and segment "e" feed into the same collecting vessel (not highlighted); inspection of the movie sequence during this epoch (Visualization 6) shows the sudden deceleration of flow in "g" while the cell aggregate in "e" is passing.

3.2. Distribution of decay time values in normal eyes

Figure 5 shows the distribution of decay time values recorded for data corresponding to 266 unique vessel segments in 2 normal subjects. Imaging sequences were 3.3 sec long and collected at 300 fps with 750 nm light. Figure 5(A) shows a histogram of decay time for individual pixels in the background (black), in the automatically segmented vascular network at large (blue), and for two of the outlier strategies discussed above (yellow and red). It can be seen that vessels in general were slightly darker than the background, with outlier pixels being much brighter, as expected. Figure 5(B) expresses the decay time metric averaged over each vessel (instead of per-pixel), for all vessel-epochs analysed (12,421 in total). At low flow velocities there is a clear correlation between flow velocity and decay time (as expected when flow velocity varies without a change in the size and separation of capillary contents); above approximately 2 mm/s, a plateau appears due to aliasing of flow sampled at 300 fps by this simple, single-pixel metric. However, note the extension of outlier events into this aliased range, especially outliers-to-self; this occurs because a longer packet of cells or plasma creates a unique signature that disrupts the pattern of aliasing and allows the correct decay time to be calculated.

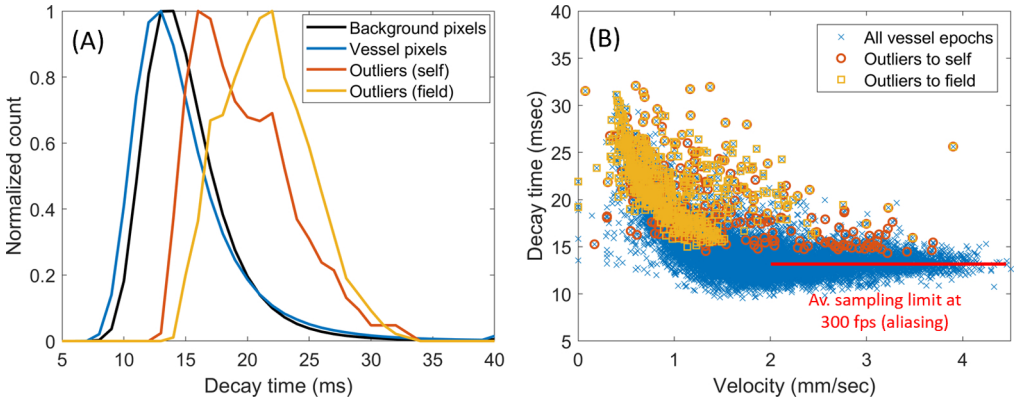

Fig. 5. Distribution of decay time values. A) Histogram of decay time for background pixels (black) and segmented vessel pixels (blue). Vessels are generally darker than background, but encounter sporadic spikes (outliers-to-self shown in red, outliers-to-field in yellow). B) Decay time for each vessel-epoch, plotted as a function of instantaneous velocity (12,421 vessel-epochs, 266 unique vessel segments). The correlation between velocity and decay time disappeared, on average, beyond ~2 mm/sec due to sampling limitations at 300 fps (red line).

3.3. Relationship of decay time to subjective assessment of capillary contents

To relate the decay time metric to the subjective impressions of an experienced observer, we manually rated instantaneous capillary contents for all outlier-flagged vessel-epochs plotted above. Control vessel-epochs were randomly interspersed to reduce bias. The results of manual evaluation of vessel-epochs are shown in Table 1. Where capillary contents were rated as "normal", data is broken down further into slow flow ($v < 1$ mm/s) and non-slowed flow ($v > 1$ mm/s).

Sensitivity of the decay time outlier approach to a subjectively identified change in capillary contents was high, with flagged outliers constituting the vast majority of "cell" (98%) and

Biomedical Optics EXPRESS

Table 1. Decay time and associated metrics together with manual categorization of capillary contents for both "outlier" and "control" vessel-epochs.

	Capillary contents			
Parameter	Cell agg. or WBC	Plasma length	Normal (v < 1 mm/s)	Normal (v > 1 mm/s)
Outlier epochs (n)	208	160	103	51
Control epochs (n)	4	14	37	340
Total epochs (n)	212	174	140	391
Rate (sensitivity or specificity)	0.98 (208/212)	0.92 (160/174)	0.74 (103/140)	0.87 (340/391)
Unique segments (n)	45	39	40	73
Velocity (mm/s for seg. in epoch)	1.8 ± 0.7	1.4 ± 0.5	0.7 ± 0.2	2.0 ± 0.8
Average velocity (mm/s for seg.)	2.0 ± 0.4	1.7 ± 0.4	0.9 ± 0.3	1.9 ± 0.7
Field velocity (mm/s in epoch)	1.9 ± 0.4	2.0 ± 0.4	1.4 ± 0.3	1.8 ± 0.4
"Sheathing" (ratio for seg. in epoch)	1.44 ± 0.38	1.38 ± 0.41	1.29 ± 0.27	1.02 ± 0.06
Average "sheathing" (ratio for seg.)	1.12 ± 0.12	1.13 ± 0.13	1.22 ± 0.24	1.01 ± 0.03

Contents were rated as "cell", "plasma" or "neither" by a blinded observer. Ratings of "neither" were broken down into slow or not-slow with a velocity criterion of 1 mm/sec. Values accompanied by uncertainty symbols indicate mean ± standard deviation.

"plasma" (92%) ratings. Sensitivity to slowed flow (as defined by an arbitrary cut-off at 1 mm/s) was lower, at 74%. Specificity was reasonably high, with 87% of ratings of "normal contents, non-slowed flow" being control epochs as opposed to outliers. Specificity could be significantly further improved by incorporating the "sheathing" index, as detailed in the Discussion.

Considering all rated vessel-epochs, the presence of a "cell" was associated with a significant reduction in flow velocity compared to the average for the same segment (paired t-test, 95% CI: −0.12 to −0.28 mm/s, $p < 1e\text{-}6$), and compared to the rest of the field at the same time (paired t-test, 95% CI: −0.07 to −0.24 mm/s, $p < 0.001$). Similarly, presence of "plasma" was associated with slowed flow compared to the segment average (paired t-test, 95% CI: −0.21 to −0.36 mm/s, $p < 1e\text{-}10$) and especially to the field average (paired t-test; 95% CI: −0.46 to −0.58 mm/s, $p < 1e\text{-}35$).

Considering all vessel-epochs together, flow was generally faster when a "cell" was present compared with "plasma" (unpaired t-test, 95% CI: +0.2 to + 0.4 mm/s, $p < 1e\text{-}6$). Flow velocity was no different on average between "cell" and "normal" contents (unpaired t-test, $p = 0.17$), but presence of "plasma" was associated with generally slower flow than for "normal" contents (unpaired t-test, 95% CI: −0.1 to −0.4 mm/s, $p < 0.01$).

As described above, to allow the outlier flagging procedure to consider the very bright decay time pixels found outside the nominal vessel lumen, we considered small contiguous clusters of pixels that were a) outliers-to-image in decay time, and b) touching the segmented vessel lumen. We recorded the proportion of extra pixels added this way for each vessel, and refer to this in Table 1 as "sheathing". The sheathing index was significantly increased compared with the vessel average where "cell" was identified (paired t-test, 95% CI for difference in the index: +27 to + 36%, $p < 1e\text{-}32$) and where "plasma" was identified (paired t-test, 95% CI: +20 to + 30%, $p < 1e\text{-}17$). During slow flow without a change in contents there was a comparatively modest increase in the sheathing index (paired t-test, 95% CI: +4 to + 10%, $p < 1e\text{-}5$); however this may have stemmed from a higher baseline amount of sheathing in these vessels (mean of 22%, as opposed to 12-13% for the vessels producing "cell" or "plasma" events).

3.4. Sample data in Type I diabetes

Figure 6 shows example data collected from young Type I diabetic subjects, none of whom had

Biomedical Optics EXPRESS

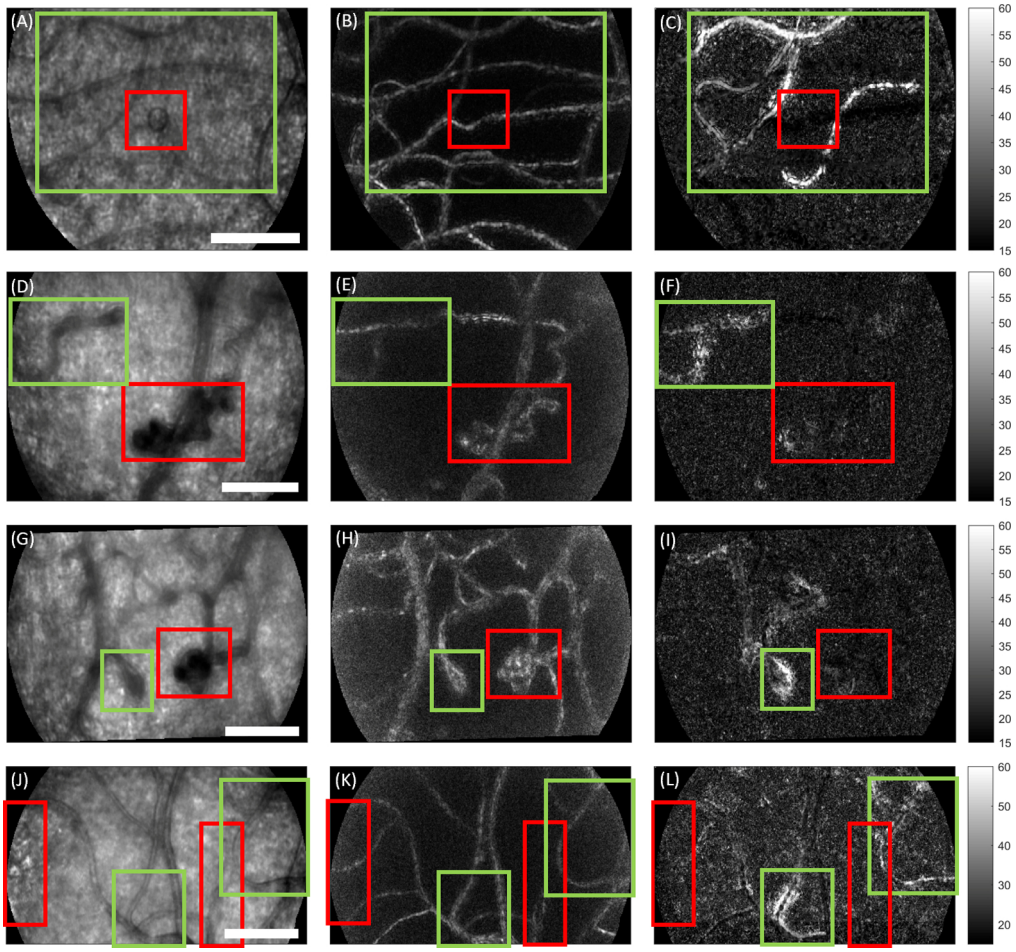

Fig. 6. Epochs of relative capillary stasis associated with sub-clinical microvascular pathology in Type I diabetes. Data collected at 200 fps with 593 nm light from 3 subjects without clinically observed retinopathy based on colour fundus photography. Each row depicts a different imaged field. Columns from left to right show mean intensity, division motion contrast, and decay time during a 100 ms epoch. Red boxes indicate the most obvious pathology in each field based on the intensity image. Green boxes show areas of relative stasis, i.e. elevated decay time. A-C) A small cyst is surrounded by several static appearing vessels, which contain long, slowly moving cell aggregates as seen in Visualization 7. D-F) A highly tortuous "knot" structure shows little elevation in decay time, but a nearby, less severe malformation does show elevated decay time. In the accompanying sequence (Visualization 8), the latter structure appears to dissipate high flow from the right into much slower flow to the left, over a very short distance. G-I) A microaneurysm is neighboured by a tight loop. Decay time appears elevated in the loop only. Accompanying sequence shown in Visualization 9. J-L) Hyperreflective spots and microvascular abnormality are seen in the vicinity of two vessels showing elevated decay time. Inspection of the accompanying sequence (Visualization 10) shows passage of long cell aggregates accompanied by extreme apparent variations in the vessel width for the vessel indicated by the left-hand green box; the vessel in the right-hand green box shows long cell aggregates undergoing extremely slow flow. Scale bars = 100 μm.

Biomedical Optics EXPRESS

any retinopathy detected by standard colour fundus photography. In each example, relative stasis of the blood column was not associated with the most obvious structural malformations, but instead in the surrounding vessels. Data was collected at 200 fps with 593 nm light over 400 ms; the bright imaging light precluded longer acquisition of data across the cardiac cycle. In the left hand column (Fig. 6(A), (D), (G), (J)) is shown the average intensity during a 100 ms epoch; in the middle column (Fig. 6(B), (E), (H), (K)), the motion contrast (division) image; in the right hand column (Fig. 6(C), (F), (I), (L)), the decay time image during the same epoch. Red boxes indicate the region showing the most obvious structural abnormalities in the intensity image. Accompanying Visualizations 7-10 provide further context. Figure 6(A)-(C) (Visualization 7) shows a small cyst which is surrounded by the passage of long, slow cell aggregates producing elevated decay time. Figure 6(D)-(F) (Visualization 8) shows a large tortuous "knot" without elevated decay time; a nearby structure is seen to convert rapid flow from the right into "sludgy" flow over a very short distance, with concomitantly elevated decay time. Figures 6(G)-(I) (Visualization 9) show a microaneurysm positioned next to a tight vascular loop; only the latter structure shows elevated decay time. Figures 6(J)-(L) (Visualization 10) shows the edge of a hyper-reflective lesion within the foveal avascular zone (left-hand red box), and also a vessel with unusual calibre change along its length (right-hand red box). Green-highlighted vessels in this field show passage of long, slow cell aggregates together with marked apparent calibre changes over time (left), and sludgy flow (right).

4. Discussion

We have demonstrated the utility of a new metric, pixel decay time, to assist in characterization of capillary flow dynamics from high spatiotemporal recordings of retinal microvasculature. Decay time is simple and fast to compute, which is advantageous given the generally time-consuming and technical nature of AO imaging which has precluded the widespread study of retinal capillary flow phenomena by more than a handful of research groups to date. The metric is easy to interpret as reflecting how static the blood column appears, and offers complementary information to flow velocity. Areas of significantly elevated decay time are comparatively rare, arising and propagating across the field where the blood column appears static due to low haematocrit, the passage of a white cell or red cell aggregate, an increase in the length of existing aggregates, and/or generally slowed flow accompanying either local variation in capillary contents or "traffic" in the surrounding network. Each of these events could have significant impacts on the local efficiency of metabolic exchange with tissue and may become more frequent or more pronounced early in the development of microvascular pathology. In otherwise normal eyes, the relative paucity of significantly elevated decay time events means that extreme values have a good chance of indicating an "interesting" flow phenomenon worthy of further investigation.

The new metric also has merit for the study of pathological flow. Clinical studies at present are limited by the difficulty and time-consuming nature of accurately mapping the vascular network, especially in the case of microstructural pathology which will not typically be well described by a "vesselness" filter [35]. Being a single-pixel measure, decay time could be used to quantify the overall degree of abnormality in a wider field without the need for vascular segmentation at all, flagging areas and epochs for further analysis if required. Also relevant to the study of vascular pathogenesis is the possibility that decay time could better reflect the capacity for metabolic exchange than velocity does alone, since it reflects both the rate of flow and the haematocrit. Thus decay time has some merit as an outcome measure in clinically oriented studies. Whilst it was shown that the decay time signal sampled at 300 fps became aliased at moderate to fast flow speeds, causing a "flatline" appearance, when capillary contents became sufficiently long and/or slow the aliasing disappeared and a clear peak was seen to "rise out" of the flatline. Hence, lower frame rate and/or wider field systems which may be employed in clinical trials may still correctly identify the most important examples of relative vascular stasis using the decay time

Biomedical Optics EXPRESS

metric. Although theoretically feasible, future studies will be required to learn whether clinical application is a practical extension of the technique described here. A key comparator will be the ability of the new metric to offer information not already accessible by OCT angiography.

A key insight made apparent with the decay time metric was that, especially during a change in capillary contents, there was an extended area of relative stasis in the image extending several microns beyond the "classical" vessel lumen (as demarcated from the division motion contrast image). We have referred to this phenomenon as "sheathing". Sheathing does not appear to have been noted in the past: relative to pixels within the lumen proper, the contrast is low and so is the temporal frequency. The low temporal frequency goes some way to explain the generally "cleaner" vessel edges obtained by division [2] as opposed to standard deviation [1] methods of perfusion mapping; the division method focuses on inter-frame changes, i.e. imposes some temporal filter on the data, whilst the standard deviation method retains all variance which includes the "sheath" (and accordingly can often result in a less "clean" looking vessel edge).

Sheathing may arise due to changes in capillary contents producing physical variations in the functional vessel diameter and/or associated, anchored connective tissue (i.e. a mechanical explanation). For example, the blood column is typically flanked by a cell-free layer of plasma and endothelial glycocalyx whose normal width is approximately 10% of that of the capillary lumen [36], but which is generally held to be highly compressible [37]. The higher values for the sheathing index which were reported here for slow vessels with normal-appearing contents, point at least in part to a mechanical, pressure-driven explanation. Alternately, or perhaps in addition, sheathing may have an optical explanation whereby the refractive index differences between various blood constituents result in oblique scatter such that light bleeds into neighbouring pixels. Confocal methods capable of manipulating the illumination geometry may be better equipped to settle this outstanding question; other strategies may include dual-plane and/or dual-wavelength acquisition to better differentiate changes in contrast occurring due to scatter from those due to defocus phase contrast.

In some cases the computed decay time metric, coupled with velocity information, could theoretically be used to infer the local haematocrit. This will be successful only in cases where the energy corresponding to the regular alternating passage of cells and plasma is the dominant source of variation in the power spectrum for a given pixel. For example, if no cells pass during the epoch in question (only plasma is present), noise sources such as fluctuations in underlying cone intensity and shot noise will dominate and the decay time image may not appear different from background. If instead a sufficient number of cells, with sufficiently high contrast, pass then the power spectrum will become dominated by their frequency of passage. Thus the decay time metric is somewhat dependent upon the size of the epoch chosen, the plane of focus, the wavelength, the power of the illumination, efficiency of reflection from the fundus, the noise characteristics of the camera, etc. These considerations may help explain the observation for some vessels above (e.g. Figure 2(F), 3(E)) that the computed decay time within the centre of the lumen was not elevated at all despite subjective confirmation of a long, slowed object moving through it. An alternate explanation for such observations could be that the apparent position of the vessel on the motion contrast image is erroneously shifted by a small amount from its true position (e.g. due to "shadowing" such as that seen in Fig. 2(C)), however, this explanation appears less likely due to the generally symmetrical appearance of the sheathing phenomenon.

The astute reader may have noted that the scale chosen for display of 300 fps data in Figs. 2, 3 and 4 was different (10–40 ms) from that chosen for the 200 fps data in Fig. 6 (15–60 ms). The difference in scaling was selected to account for the dependence of the centroid of the power spectrum on the sampling rate. For a strictly white noise process, the centroid lies simply half-way through the measurable range; this means, for example, that doubling the frame rate is expected to halve the average decay time for the background which is dominated by shot noise. In other words, increasing the frame rate will shift the lower end of the decay time scale upwards. We

Biomedical Optics EXPRESS

also shifted the upper end of the scale in the same proportion for the displayed images, in order to maintain the same dynamic range (in this case, 4:1) so that images appear visually similar.

The decay time metric represents the frequency of intensity variations at a pixel, rather than the degree or sign of relative contrast. This is useful since a large fraction of the contrast (at 750 nm, almost all of the contrast) is generated by defocused phase contrast, i.e. by differences in refractive index interacting with separation from the plane of focus [34]. Specifically, in our sequences cells which are anterior to focus appear darker than the background and plasma, whilst cells posterior to focus appear brighter (reversed sign of contrast). Similarly, use of a frequency-based metric should provide some robustness to wavelength-dependent absorption shifts (e.g. haemoglobin absorbs more strongly at 593 nm, which was used to acquire the data shown in Fig. 4), as long as the passage of cellular material remains the dominant source of variance through time.

The dependence of the decay time metric on the parameters described above mean that the significance of a particular value for the decay time metric is somewhat specific to the particular system and acquisition parameters. Values are also liable to change according to any inclination of the vessel axis with respect to the imaging plane (e.g. "diving" capillaries). This lends credence to the analysis approach adopted here, which does not impose a particular threshold for a significant elevation in decay time but instead focuses on relative changes by a) taking into account what a particular vessel is doing relative to the field, to itself and to other vessels of similar velocity; and b) focusing on outliers with respect to these considerations. Perhaps a criterion can be developed that is less sensitive to imaging parameters; identifying local peaks (as opposed to centroids) of the power spectrum, appropriately filtered, may be a fruitful avenue in this regard (though we note that images produced in this way do not appear to vary as "naturally" as with the centroid method).

As described above, the presence of one or more outliers tended to indicate higher quality data, with fewer outlier-containing vessels being rejected due to low quality compared with non-outlier vessels. This self-selection for quality generally supports the utility of an outlier strategy and supports the notion that when an outlier is flagged, there is likely to be an event that is worthy of further investigation.

The outlier analysis shown in Table 1 revealed that 13% of the "normal contents, non-slowed flow" events were flagged as outliers (i.e. specificity was 87%). Upon manual review of these seeming misclassifications, the vast majority occurred due to aliasing, which arises when the local rate of cell passage interacts unfavourably with the frame rate such that erroneous standstill or slight reversal in flow appears. The specific frame rate at which aliasing occurs will depend on the moment-to-moment configuration of cells within the capillary tube; the on-average limitation was depicted in Fig. 5 by the red line extending beyond ~2 mm/s. Since aliasing does in fact create the illusion of stasis in the video sequence, we do not regard the falsely identified outliers as a primary limitation of the decay time metric *per se*, but rather of the imaging frame rate at 300 fps. Recent work has argued that imaging at 400 fps may be required to non-ambiguously assay normal flow in all the retinal capillaries [31], however the requirement should be higher for a simplistic, single-pixel measure as developed here.

We previously described the pixel intensity cross-correlation ("PIX") method, employed here for velocimetry, as being comparatively robust to aliasing [29]; this is confirmed by the ability seen here to faithfully track variations with the cardiac cycle at flow velocities which were rapid enough to cause "flatline" of the decay time measure. Given the robustness of the velocimetry algorithm, it may be possible to account for the influence of aliasing, i.e. to "resample" the sequence and so estimate the true decay time. In lieu of this, aliasing could be combated with a faster frame rate as mentioned, or by looking for reversals of flow velocity and/or sudden changes in the apparent lengths of cells.

Biomedical Optics EXPRESS

Despite the limitations described above, errors in classification were much lower when considering epochs identified as containing cell aggregates and/or plasma. This is because aliasing depends critically on both the uniformity of the cell (or plasma) column and the spacing between cells. A temporary disruption to these parameters caused by, for example, a passing long aggregate of red cells, is easy to observe in the flow sequences and allows the true direction of flow to be determined and accordingly, the true decay time to be calculated during that epoch.

Another way to discriminate spuriously elevated decay time from true stasis is to consider the "sheathing" phenomenon described above. One would not expect the sheathing index, which results from either physiological differences in the position of the vessel boundary and/or refractive index differences between cells, to be elevated during a pseudo-standstill that was simply a result of aliasing. The sheathing index in the correctly classified outliers of our data averaged 30%, versus only 5% in the misclassified ones; this difference was highly significant (unpaired t-test, 95% CI on the difference of 18-31%, $p < 1e\text{-}11$). Thus the specificity of the high decay time events may be greatly enhanced, simply by determining whether the pixels in the immediate neighbourhood of the vessel were also elevated.

Mis-matches between the outlier procedure and subjective review of capillary contents may also have resulted because the grader was provided only with a 200 ms snapshot surrounding the epoch in question, making it difficult to recognise aliasing which manifests in the wider sequence as acceleration followed by sudden cessation and reversal of flow. In addition, the grader applied a criterion that the capillary contents during the brief sample epoch looked unusual relative to their own impression of a typical vessel; thus an event could be missed that should be considered generally normal, but could be highly abnormal for a particular vessel (i.e. an outlier-to-self). It is impossible to resolve such conflicts at present, i.e. to determine what really does constitute a significant departure from normal, pending the formation of a theory which accurately describes normal capillary network flow patterns. However, the identification and according explanation of rare events with the potential to significantly impact metabolic exchange should be considered a requirement of such a theory; as should relative variations in pressure which may contribute to the "sheathing" phenomenon described above. Hence, the proposed metric appears to offer a useful investigative tool to further exploration of the laws governing capillary network flow. Useful questions to address will include the role of vessel diameter, tortuosity, branch angle/order, and depth of the capillary plexus, and how these interact with the velocity, haematocrit, proportion of oxygenated haemoglobin, passage of white cells, presence of the "sheathing" phenomenon observed here, etc.

The diabetic data presented in Fig. 6 show that the decay time metric may be useful in identifying regions of functional deficit in the vascular network. Although the data is limited and not powered nor designed to reveal statistical differences compared with normals, it shows that severe structural abnormalities need not be associated with severe flow abnormalities (and vice versa). Several speculative theories present themselves which require careful longitudinal study: perhaps some instances of structural adaptation seen in diabetic vessels serve in fact to restore a semblance of normal flow; perhaps they help to redirect flow away from the affected parts of the network into surrounding vessels; perhaps the presence of abnormal flow patterns drives the development of future structural abnormalities.

Funding

Australian Research Council (DP180103393).

Disclosures

The authors declare no conflicts of interest.

Biomedical Optics EXPRESS

References

1. T. Y. Chui, Z. Zhong, H. Song, and S. A. Burns, "Foveal avascular zone and its relationship to foveal pit shape," Optometry Vision Sci. **89**(5), 602–610 (2012).
2. J. Tam, J. A. Martin, and A. Roorda, "Noninvasive visualization and analysis of parafoveal capillaries in humans," Invest. Ophthalmol. Visual Sci. **51**(3), 1691–1698 (2010).
3. S. Arichika, A. Uji, M. Hangai, S. Ooto, and N. Yoshimura, "Noninvasive and direct monitoring of erythrocyte aggregates in human retinal microvasculature using adaptive optics scanning laser ophthalmoscopy," Invest. Ophthalmol. Visual Sci. **54**(6), 4394–4402 (2013).
4. P. Bedggood and A. Metha, "Direct visualization and characterization of erythrocyte flow in human retinal capillaries," Biomed. Opt. Express **3**(12), 3264–3277 (2012).
5. A. Guevara-Torres, A. Joseph, and J. Schallek, "Label free measurement of retinal blood cell flux, velocity, hematocrit and capillary width in the living mouse eye," Biomed. Opt. Express **7**(10), 4228–4249 (2016).
6. J. Tam and A. Roorda, "Speed quantification and tracking of moving objects in adaptive optics scanning laser ophthalmoscopy," J. Biomed. Opt. **16**(3), 036002 (2011).
7. C. Berry, N. Sidik, A. C. Pereira, T. J. Ford, R. M. Touyz, J. C. Kaski, and A. H. Hainsworth, "Small-Vessel Disease in the Heart and Brain: Current Knowledge, Unmet Therapeutic Need, and Future Directions," J. Am. Heart Assoc. **8**(3), e011104 (2019).
8. F. Bosetti, Z. S. Galis, M. S. Bynoe, M. Charette, M. J. Cipolla, G. J. Del Zoppo, D. Gould, T. S. Hatsukami, T. L. Jones, and J. I. Koenig, ""Small Blood Vessels: Big Health Problems?": Scientific Recommendations of the National Institutes of Health Workshop," J. Am. Heart Assoc. **5**(11), e004389 (2016).
9. N. B. Hamilton, D. Attwell, and C. N. Hall, "Pericyte-mediated regulation of capillary diameter: a component of neurovascular coupling in health and disease," Front. Neuroenerg. **2**, 5 (2010).
10. G. P. Rodgers, A. N. Schechter, C. T. Noguchi, H. G. Klein, A. W. Nienhuis, and R. F. Bonner, "Periodic microcirculatory flow in patients with sickle-cell disease," N. Engl. J. Med. **311**(24), 1534–1538 (1984).
11. T. Luo, T. J. Gast, T. J. Vermeer, and S. A. Burns, "Retinal vascular branching in healthy and diabetic subjects," Invest. Ophthalmol. Visual Sci. **58**(5), 2685–2694 (2017).
12. S. A. Burns, A. E. Elsner, T. Y. Chui, D. A. VanNasdale, C. A. Clark, T. J. Gast, V. E. Malinovsky, and A.-D. T. Phan, "In vivo adaptive optics microvascular imaging in diabetic patients without clinically severe diabetic retinopathy," Biomed. Opt. Express **5**(3), 961–974 (2014).
13. J. Tam, K. P. Dhamdhere, P. Tiruveedhula, S. Manzanera, S. Barez, M. A. Bearse, A. J. Adams, and A. Roorda, "Disruption of the retinal parafoveal capillary network in type 2 diabetes before the onset of diabetic retinopathy," Invest. Ophthalmol. Visual Sci. **52**(12), 9257–9266 (2011).
14. S. Arichika, A. Uji, S. Ooto, Y. Muraoka, and N. Yoshimura, "Effects of age and blood pressure on the retinal arterial wall, analyzed using adaptive optics scanning laser ophthalmoscopy," Sci. Rep. **5**(1), 12283 (2015).
15. J. G. Hillard, T. J. Gast, T. Y. Chui, D. Sapir, and S. A. Burns, "Retinal arterioles in hypo-, normo-, and hypertensive subjects measured using adaptive optics," Trans. Vis. Sci. Tech. **5**(4), 16 (2016).
16. M. Lombardo, M. Parravano, S. Serrao, P. Ducoli, M. Stirpe, and G. Lombardo, "Analysis of retinal capillaries in patients with type 1 diabetes and nonproliferative diabetic retinopathy using adaptive optics imaging," Retina **33**(8), 1630–1639 (2013).
17. D. Rosenbaum, A. Mattina, E. Koch, F. Rossant, A. Gallo, N. Kachenoura, M. Paques, A. Redheuil, and X. Girerd, "Effects of age, blood pressure and antihypertensive treatments on retinal arterioles remodeling assessed by adaptive optics," J. Hypertens. **34**(6), 1115–1122 (2016).
18. M. Dubow, A. Pinhas, N. Shah, R. F. Cooper, A. Gan, R. C. Gentile, V. Hendrix, Y. N. Sulai, J. Carroll, and T. Y. Chui, "Classification of human retinal microaneurysms using adaptive optics scanning light ophthalmoscope fluorescein angiography," Invest. Ophthalmol. Visual Sci. **55**(3), 1299–1309 (2014).
19. J. Lammer, S. G. Karst, M. M. Lin, M. Cheney, P. S. Silva, S. A. Burns, L. P. Aiello, and J. K. Sun, "Association of Microaneurysms on Adaptive Optics Scanning Laser Ophthalmoscopy With Surrounding Neuroretinal Pathology and Visual Function in Diabetes," Invest. Ophthalmol. Visual Sci. **59**(13), 5633–5640 (2018).
20. T. Y. Chui, S. Mo, B. Krawitz, N. R. Menon, N. Choudhury, A. Gan, M. Razeen, N. Shah, A. Pinhas, and R. B. Rosen, "Human retinal microvascular imaging using adaptive optics scanning light ophthalmoscopy," Int. J. Retin. Vitr. **2**(1), 11 (2016).
21. T. Y. P. Chui, A. Pinhas, A. Gan, M. Razeen, N. Shah, E. Cheang, C. L. Liu, A. Dubra, and R. B. Rosen, "Longitudinal imaging of microvascular remodelling in proliferative diabetic retinopathy using adaptive optics scanning light ophthalmoscopy," Ophthalmic Physiol. Opt. **36**(3), 290–302 (2016).
22. A. Pinhas, M. Razeen, M. Dubow, A. Gan, T. Y. Chui, N. Shah, M. Mehta, R. C. Gentile, R. Weitz, and J. B. Walsh, "Assessment of perfused foveal microvascular density and identification of nonperfused capillaries in healthy and vasculopathic eyes," Invest. Ophthalmol. Visual Sci. **55**(12), 8056–8066 (2014).
23. J. Tam, P. Tiruveedhula, and A. Roorda, "Characterization of single-file flow through human retinal parafoveal capillaries using an adaptive optics scanning laser ophthalmoscope," Biomed. Opt. Express **2**(4), 781–793 (2011).
24. S. Arichika, A. Uji, T. Murakami, N. Unoki, S. Yoshitake, Y. Dodo, S. Ooto, K. Miyamoto, and N. Yoshimura, "Retinal hemorheologic characterization of early-stage diabetic retinopathy using adaptive optics scanning laser ophthalmoscopy," Invest. Ophthalmol. Visual Sci. **55**(12), 8513–8522 (2014).

Biomedical Optics EXPRESS

25. Z. Burgansky-Eliash, A. Barak, H. Barash, D. A. Nelson, O. Pupko, A. Lowenstein, A. Grinvald, and A. Rubinstein, "Increased retinal blood flow velocity in patients with early diabetes mellitus," Retina **32**(1), 112–119 (2012).
26. Z. Burgansky-Eliash, D. A. Nelson, O. P. Bar-Tal, A. Lowenstein, A. Grinvald, and A. Barak, "Reduced retinal blood flow velocity in diabetic retinopathy," Retina **30**(5), 765–773 (2010).
27. A. Duan, P. A. Bedggood, B. V. Bui, and A. B. Metha, "Evidence of flicker-induced functional hyperaemia in the smallest vessels of the human retinal blood supply," PLoS One **11**(9), e0162621 (2016).
28. X. Fu, J. S. Gens, J. A. Glazier, S. A. Burns, and T. J. Gast, "Progression of diabetic capillary occlusion: a model," PLoS Comput. Biol. **12**(6), e1004932 (2016).
29. P. Bedggood and A. Metha, "Mapping flow velocity in the human retinal capillary network with pixel intensity cross correlation," PLoS One **14**(6), e0218918 (2019).
30. A. de Castro, G. Huang, L. Sawides, T. Luo, and S. A. Burns, "Rapid high resolution imaging with a dual-channel scanning technique," Opt. Lett. **41**(8), 1881–1884 (2016).
31. B. Gu, X. Wang, M. D. Twa, J. Tam, C. A. Girkin, and Y. Zhang, "Noninvasive in vivo characterization of erythrocyte motion in human retinal capillaries using high-speed adaptive optics near-confocal imaging," Biomed. Opt. Express **9**(8), 3653–3677 (2018).
32. A. Joseph, A. Guevara-Torres, and J. Schallek, "Imaging single-cell blood flow in the smallest to largest vessels in the living retina," eLife **8**, e45077 (2019).
33. L. G. Brown, "A survey of image registration techniques," ACM Comput. Surv. **24**(4), 325–376 (1992).
34. P. Bedggood and A. Metha, "Analysis of contrast and motion signals generated by human blood constituents in capillary flow," Opt. Lett. **39**(3), 610–613 (2014).
35. T. Jerman, F. Pernuš, B. Likar, and Ž. Špiclin, "Beyond Frangi: an improved multiscale vesselness filter," in *Medical Imaging 2015: Image Processing*, (International Society for Optics and Photonics, 2015), 94132A.
36. H. Vink and B. R. Duling, "Identification of distinct luminal domains for macromolecules, erythrocytes, and leukocytes within mammalian capillaries," Circ. Res. **79**(3), 581–589 (1996).
37. S. Reitsma, D. W. Slaaf, H. Vink, M. A. Van Zandvoort, and M. G. Oude Egbrink, "The endothelial glycocalyx: composition, functions, and visualization," Pfluegers Arch. **454**(3), 345–359 (2007).